Journal of Colloid and Interface Science 623 (2022) 646–659

Contents lists available at ScienceDirect

Journal of Colloid and Interface Science

journal homepage: www.elsevier.com/locate/jcis

Performance of a C-containing Cu-based photocatalyst for the degradation of tartrazine: Comparison of performance in a slurry and CPC photoreactor under artificial and natural solar light

Paula Muñoz-Flores [a,b,*], Po S. Poon [a], Conchi O. Ania [c,*], Juan Matos [d,*]

[a] Unidad de Desarrollo Tecnológico (UDT), Universidad de Concepción, Barrio Universitario s/n, Concepción, Chile
[b] Facultad de Ingeniería, Universidad de Concepción, Barrio Universitario s/n, Concepción, Chile
[c] CEMHTI, CNRS (UPR 3079), Université d'Orléans, 45071 Orléans, France
[d] Instituto de Ciencias Químicas Aplicadas, Facultad de Ingeniería, Universidad Autónoma de Chile, 8900000 Santiago, Chile

GRAPHICAL ABSTRACT

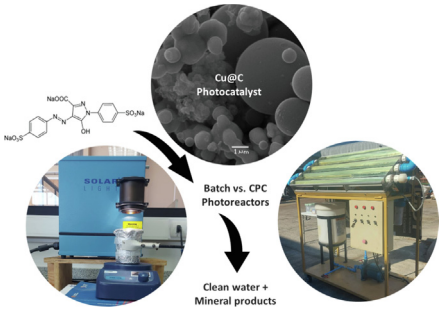

ARTICLE INFO

Article history:
Received 11 January 2022
Revised 5 May 2022
Accepted 6 May 2022
Available online 10 May 2022

Keywords:
Cu-based catalyst
Carbon
Tartrazine
Solar-driven photocatalysis
CPC photoreactor

ABSTRACT

A carbon-containing Cu-based material (Cu@C) was used as photocatalyst for the degradation of a commonly food-industry azo-dye (tartrazine, also called Y5), under solar light at laboratory and pilot scale photoreactors. Important performance parameters such as dark adsorption capacity, catalysts loading and initial concentration of the dye were first optimized in a slurry photoreactor at laboratory scale under artificial solar light following the kinetics of degradation of the dye. Afterwards, the photocatalytic activity was investigated at pilot scale in a compound parabolic collector (CPC) photoreactor operating for 10 h of irradiation. The degradation of tartrazine is among the highest values reported for alternative metal oxide semiconductors, in both photoreactor configurations. Catalytic data revealed a 3 times faster degradation kinetics of tartrazine in the CPC photoreactor under natural solar light than in the slurry reactor under artificial solar light. This behavior indicates that a moderate photon flux in the CPC is more adequate to operate with the prepared photocatalyst, as it minimizes the recombination of charge carriers in the catalyst. This is important, since most of the photocatalytic tests designed to evaluate the activity of novel materials are frequently carried out under simulated solar light and disregard the impact of photon flux in outdoor conditions.

* Corresponding authors at: Unidad de Desarrollo Tecnológico (UDT), Universidad de Concepción, Barrio Universitario s/n, Concepción, Chile (P. Muñoz-Flores); CEMHTI, CNRS (UPR 3079), Université d'Orléans, 45071 Orleáns, France (Conchi O. Ania); Instituto de Ciencias Químicas Aplicadas, Facultad de Ingeniería, Universidad Autónoma de Chile, 8900000 Santiago, Chile (Juan Matos).
E-mail addresses: paulamunozf@udec.cl (P. Muñoz-Flores), conchi.ania@cnrs-orleans.fr (C.O. Ania), juan.matos@uautonoma.cl (J. Matos).

https://doi.org/10.1016/j.jcis.2022.05.042
0021-9797/

1. Introduction

During the past centuries, the industrial activities have caused a notable environmental damage as a result of the release of toxic organic and inorganic compounds in the environment, and particularly to water effluents [1–3]. An example is seen in the remarkable increase in the concentration of some dyes and azo-dyes (e.g., tartrazine) in wastewaters derived from the food industry. The development of global policies for the efficient treatment of these pollutants has become an important challenge nowadays [4]. In this regard, conventional wastewater treatments are mostly based on physical, chemical, and biological processes, and azo-dyes are either not biodegradable or following a slow kinetics [5–7]. Thus, new strategies are needed to assure their degradation, and to produce clean water at a lower cost.

Advanced oxidation processes (AOPs) are recognized as effective solutions for the degradation of emerging pollutants from wastewater [8–10]. The common characteristic of such processes is the production of hydroxyl radicals (·OH), which are capable to oxidize and mineralize almost any organic molecule, producing CO_2, water and mineral products [11,12]. Among AOPs, heterogeneous photocatalysis has long been investigated in the last decades [8,9,13,14] as it is a low-cost, eco-friendly, and sustainable treatment technology. Since it is based on the interaction of light with a photoactive semiconductor, one of its main advantages is the possibility to use solar irradiation as energy source [13].

Nowadays, TiO_2 is considered the benchmark photocatalyst under UV light [8,9,14] due to its adequate electronic energy bandgap (3.2 eV), chemical stability and low cost. However, its low photoactivity under visible light along with some other disadvantages [14,15] related to the recovery and reuse have limited its large-scale implementation in solar processes [16,17]. Consequently, the search for photocatalysts based on metallic semiconductors remains an open topic for investigation.

Among the transition metals, copper-based materials are widely investigated in many fields of application [18–29]. For instance, Cu-based oxides have been successfully used in transistors [18], spintronic devices [19], supercapacitors [20], as photocatalysts [21,26–29], gas sensing [22], electrochromic devices [23], or as transparent conducting oxides [24]. Particularly, copper oxides are non-toxic, low-cost, and abundant semiconductors with energy bandgap values [25,26] between 1.2–1.7 eV for CuO and 1.9–2.4 eV for Cu_2O, which makes them interesting candidates for photocatalytic applications under natural solar light. As a few examples, it has been reported that copper oxide catalyzes the photodegradation of organic pollutants such as phenol [28], and different types of dyes including methyl orange [21], methylene blue [27] and tartrazine [29].

However, most photocatalytic studies are carried out at lab-scale using artificial solar light, which makes necessary to investigate the scaling up of the process by applying realistic illumination conditions (natural sunlight) in large-scale photoreactors. A relevant aspect in water treatment applications under solar irradiation is the choice of the photoreactor, being compound parabolic collector (CPC) solar photoreactors among the best alternatives in wastewater purification and disinfection applications as they are very efficient collecting solar photons and easy to use [30–32]. In addition, they require little capital investment and can be manufactured in different sizes, which allows versatility in their installation [30–32].

Considering all this, the aim of this work was to explore the feasibility of the use of a carbon containing Cu-based photocatalyst for the degradation of tartrazine under solar light at pilot scale using a compound parabolic collector (CPC) photoreactor. The photocatalyst was selected based on our previous study demonstrating its good photocatalytic activity under solar light, its stability against lixiviation, and its availability (e.g., copper is an abundant raw element in Chile and the search for novel applications for copper-based materials has become of great interest for the mining industry) compared to other metallic photocatalysts [29]. On the other hand, tartrazine is an azo-dye commonly found in wastewaters from food industry; the removal and control of food additives for the azo-dye family is receiving increasing attention due to some controversies on their toxicity. For these reasons, we have carried out a comparative study of the catalytic performance of a carbon-containing copper-based photocatalyst under artificial solar light in a conventional slurry photoreactor and under natural solar light in a CPC photoreactor. A preliminary optimization of some key catalytic performance parameters (catalysts loading, dye initial concentration) was conducted at lab-scale using artificial solar light, before exploring the performance at large scale in a semi-industrial CPC photoreactor in outdoor irradiation conditions.

2. Experimental

2.1. Synthesis of the photocatalyst

The carbon-containing Cu-based photocatalyst was prepared following a two-step procedure, using furfural ($C_5H_4O_2$, 98.5%, Sigma-Aldrich) as carbon source and copper (II) acetylacetonate [$Cu(O_2C_5H_7)_2$, 99.0%, Merck) as copper precursor. Furfural was chosen as the carbon source due to its low flash point that favors the control of coalescence mechanisms yielding homogenous spherical particles [33]. The synthesis has been reported elsewhere [29]; briefly, he precursor was dissolved in absolute ethanol (C_2H_6O, 99.5%, Merck), introduced in a Teflon-lined autoclave and heated to 180 °C for 16 h. The temperature was chosen based on our previous experience, to assure a fast degradation/evaporation of carbon atoms from furfural precursor [29,33–35]. The solid obtained after the solvothermal treatment was filter out, washed in ethanol, and further stabilized by pyrolysis at 800 °C for 2 h under N_2 flux (100 mL min^{-1}). The resulting material was labelled as Cu@C [29].

2.2. Characterization techniques

The moisture, inorganic content and the fixed carbon were obtained from a thermogravimetric approach. The moisture content was determined from the mass loss of the sample after two hours at 100 °C under static air. On the other hand, the inorganic content was obtained from the remaining weight after calcining the sample at static air within a ceramic muffle at 550 °C by 16 h, and the remaining fraction corresponds to the fixed carbon content, after subtracting the moisture.

The surface pH of the catalyst was measured using the pH-drift procedure described elsewhere [36]. Briefly, different masses of the catalyst powders were added to 25 mL distilled water and the pH of the suspension was followed under stirring until constant pH. The pH was measured on a portable pH meter-ORP model 8601D calibrated with buffers of pH ca. 4, 7 and 10. The values of constant pH are plotted as a function of the weight of the catalyst, and the surface pH was taken as the value in the steady-state condition.

The porosity of the catalyst was characterized by measuring the N_2 adsorption/desorption isotherm at −196 °C in a volumetric analyzer (Micromeritics, Tristar). The catalyst was outgassed at 120 °C for 17 h before analysis. The gas adsorption data was used to evaluate the specific surface area (S_{BET}) using the Brunauer–Emmet–Teller equation, the total pore volume (V_{total}) at a relative pressure of 0.99, and the micropore volume (V_{micro}) using the Dubinin–Radushkevich (DR) formulism [37].

Diffuse reflectance UV–visible spectra (DR/UV–vis) of the catalyst was registered in a UV–vis–NIR Varian spectrophotometer (model Cary 5000) equipped with an integrating sphere and using $BaSO_4$ as standard of reference. The spectra were recorded using a wavelength range between 220 and 700 nm in the diffuse reflectance modes and the data was transformed to a magnitude proportional to the extinction coefficient using the Kubelka-Munk function, $F(R\infty)$. Spectra were collected at 1 nm intervals with a spectral bandwidth of 2 nm. Powders of the catalyst were pressed in holders of ca. 3 cm diameter and 5 mm depth.

X-ray diffraction patterns were recorded on a Bruker diffractometer (model D4 ENDEAVOR) with CuKα radiation. Measurements were carried out in the range 3–70°, with a scanning step of 0.02° and a fixed counting time of 10 s. Mean size of crystallites (D) were obtained by Scherrer's formula (Eq. (1)):

$$D = \frac{K.\lambda}{\beta \cdot \cos\theta} \quad (1)$$

with K = 0.89, λ = 0.154178 nm, and β corresponds to the FWHM (full width at half maximum of the peak's intensity) in radians at the diffraction angle θ. The crystalline phases composing the catalyst were identified by the JCPDS number cards, according to the International Centre for Diffraction Data [38,39].

The morphology of the catalyst was verified by scanning electron microscopy (SEM) using a microscope JEOL model JSM 6380LV with an energy dispersive X-ray detector (EDS) from Oxford instrument working at 10 mm and operating at 20 kV. Transmission electron microscopy (TEM) was performed in a microscope JEOL JEM 1200EX II2, operating at 100 kV, containing a GATAN camera and the electron diffraction (ED) pattern was taken to verify the degree of crystalline structure of the catalyst.

2.3. Photocatalytic tests under artificial solar light in a slurry batch reactor

Initial photocatalytic studies for the degradation of tartrazine ($C_{16}H_9N_4Na_3O_9S_2$, 85% purity, Sigma Aldrich, molecular weight 534.36 g mol^{-1}) were performed in a slurry photoreactor under artificial solar light provided by a solar simulator (SOLAR® Light, LS-1000 Series, 1950 $W{\cdot}m^{-2}$). The goal is to optimize some key photocatalytic operating parameters such as the catalysts loading and the initial concentration of the dye before evaluating the performance in the CPC photoreactor under natural sunlight. A series of photocatalytic tests were carried out at loadings ranging from 0.25 – 1.0 g L^{-1} (ca. 31.3, 62.5, 93.75 and 125 mg of catalysts in 125 mL of Y5 solution) for an initial concentration of 5 ppm of the dye (ca. 9.4 μmol L^{-1}). In a second set of experiments, the optimized catalyst loading was selected to evaluate the impact of the initial concentration of the dye (with values ranging from ca. 5–15 ppm, corresponding to 9.4–28.2 μmol L^{-1}). All the photocatalytic tests were performed at 25 °C in a cylindrical flask (Pyrex, total volume ca. 250 mL) and open to air. Before irradiation, the catalysts/solution suspensions were allowed to equilibration in dark conditions for 60 min. This time was selected based on the preliminary adsorption studies of the dye to allow more than 90% of pollutant to be adsorbed in the catalyst [29]. After this time, the suspensions were irradiated for 7 h in the solar simulator. All the adsorption and photocatalytic experiments were performed at least by duplicate, with errors lower than 5% in all cases.

2.4. Photocatalytic tests in a flow CPC solar photoreactor

After the optimization of the catalyst loading and initial concentration, the potential application of the Cu@C catalyst for the degradation of the azo-dye was evaluated under real solar irradiation. To do so, photocatalytic tests were performed in a pilot plant equipped with concentrating parabolic collector (CPC) photoreactor of ca. 1 m^2 of solar exposition area. A complete description of the pilot plant has been reported elsewhere [40] and a summary of the properties of the CPC photoreactor are compiled in Table S1 (supplementary material, SM). The solar radiation during the experiments was measured with a pyranometer (Solar Light, model PMA2144). Experiments were performed on a 2 ppm (3.7 μmol L^{-1}) solution of Y5 (total volume 20 L), added to a tank in the CPC photoreactor; the tank was covered with a solar shield to avoid indirect bleaching of the dye. Before adding the catalyst, the solution of the dye was allowed to flow for 30 min in the system for a correct homogenization. Afterwards, a loading of 0.25 g L^{-1} Cu@C was incorporated in the suspension, keeping the system under dark conditions for 90 min to achieve adsorption equilibrium. After the dark equilibration, the CPC photoreactor was exposed to natural solar irradiation. Aliquots were collected at regular intervals and the kinetics of the photocatalytic degradation of Y5 was followed as a function of residence time (t_R) in the reactor. According to a previous work [40], the residence time is proportional to the experimental time (t) regardless the flow rate, according to the following expression: $t_R = t(V_{Irr}/V_{Tot})$, where a V_{Irr} is the irradiated volume (9.5 L) and V_{Tot} the total volume of the suspension (20 L). All the photocatalytic tests in the CPC were performed at least by duplicate; errors obtained were in all the cases lower than 5%.

2.5. Photocatalytic tests in the presence of scavengers

Reactive oxygen species (ROS) were evaluated by addition of benzoquinone (BQ, Sigma-Aldrich, purity ≥ 99%) and isopropyl alcohol (IPA, Sigma-Aldrich, purity 99.7%) as scavengers for the capture of superoxide radical ($\cdot O_2^-$) and hydroxyl radical (·OH), respectively. The experimental conditions for the scavenger tests using the CPC photoreactor were as follows. An aqueous solution of Y5 containing 2 ppm of the dye was prepared (ca. 19.7 L) and mixed with 0.3 L of IPA, or 120 mg of BQ. The solution was put in contact with a catalysts loading of 0.25 g L^{-1}, and the photocatalytic test was performed as indicated above. Data corresponding to the slurry photoreactor has been reported in our previous study [29]; we herein reintroduce the results for comparison purposes. Results were compared with those observed in absence of scavengers.

2.6. Analytical techniques

The concentration of the dye was measured by UV–vis spectroscopy (Perkin Elmer, UV–vis Lambda 365) at 426 nm. During the photocatalytic assays, aliquots of 2.5 mL of the solution were taken out and filtered (0.45 μm PVDF filter) before analysis.

The total carbon (TC) was measured with a Shimadzu TOC-VCSN analyzer to compare the efficiency in the mineralization of the dyes in both photoreactors and irradiation conditions. Aliquots of the dye were analyzed after 1 h in dark conditions and during irradiation.

The lixiviation of copper species from the catalyst to the solution upon the photocatalytic tests was monitored by a semiquantitative analysis using colorimetric test strip standards for copper (Mquant Merck 1.10003.001) as reported elsewhere [29]. Quantitative analyses were also performed by UV spectrophotometry of Cu (II) in solution at 290 nm, using high-purity Cu $(acac)_2$ as internal standard.

3. Results and discussion

We have carried out a comparative study of the catalytic performance of a carbon-containing copper-based material under artificial solar light in a conventional slurry photoreactor and under outdoor solar irradiation in a pilot scale CPC photoreactor. The photocatalyst used in this study was selected based on a previous study reporting its photocatalytic activity for the degradation of tartrazine, as well as its high chemical stability and resilience to lixiviation of the photoactive copper species. Details about the synthesis and characterization have been described in our previous work [29]; we herein reintroduce certain elements of the characterization for interpretation of the photocatalytic activity.

3.1. Characterization of the photocatalyst

A carbon-containing copper-based material was obtained by a two-step procedure (hydrothermal reaction at 180 °C followed by pyrolysis at 800 °C) using furfural and copper (II) acetylacetonate as precursors. The yield of the synthesis was ca. 23 ± 5 wt%.

The prepared Cu@C catalyst is composed by ca. 20 wt% of carbon and 80 wt% of inorganic matter; the nominal fractions of carbon, oxygen and copper are presented in Table 1. The catalyst presented a nominal carbon content slightly lower than expected, which is attributed to the consumption of a fraction of carbon atoms upon reaction with copper phases, most likely releasing gaseous species (e.g, CO_2). The interaction between the carbon atoms and the copper species during the first step of the synthesis is of great importance since it may be responsible of the intercalation of carbon atoms within the crystalline framework of Cu-based oxides phases. As seen in Fig. S1 (SM), Cu@C presented a dark gray color which is a clear indicative of the presence of an important content of carbon besides the copper phases.

Fig. 1 shows SEM images of the Cu@C catalyst, where the spherical morphology of the particles of micrometric size (average ca. 2 μm, Fig. S3, SM) can be observed. As seen, the surface of the spheres shows certain degree of roughness and a large fraction of spheres is interconnected by coalescence interfaces (marked as white arrows). Similar observations have been reported for C@TiO_2 catalysts prepared following a similar route [35]. SEM-EDS analysis of the catalyst particles in a zone rich of spheres (Fig. S2, SM) shows that the spherical particles are mainly composed of carbon (Table 1), with some copper oxides. These values differ from those of the proximate analysis (Table 1), as the later refers to the overall bulk composition.

TEM images of the catalyst (Fig. 2) evidence the symmetric spherical shape of the particles. A similar finding has been reported for C-doped TiO_2 photocatalysts [33,35], and it is attributed to the low flash point of furfural that would give rise to fast degradation reactions during the hydrothermal step.

TEM images also show the core-shell structure of certain particles with an external wall thickness of ca. 12.5 nm. This value is lower than that observed in some irregular particles located in the core (thickness up to ca. 71.4 nm, white arrows in Fig. 2). Fig. 2 also shows connected spheroidal particles (white circles) located within the main spherical shell of the structure. This suggests that coalesce is the driven-force mechanism for the formation of the catalyst's particles.

A thorough physicochemical characterization of the Cu@C catalyst is shown in the Supplementary Material (Fig. S4, SM). A summary of selected textural parameters, surface pH, optical energy gap, and crystalline parameters of Cu@C catalyst are given in Table 2.

The photocatalyst displayed a low BET surface area of ca. 90 m^2g^{-1}, with ca. 48% of micropore volume. The surface pH of the catalyst (Fig. S4, SM) is slightly acidic, which is attributed to the presence of O-containing groups in the surface of the carbon phase, and/or to the Cu-based oxides.

XRD patterns of the Cu@C photocatalyst (Fig. S4, SM) showed that the sample is composed of Cu, CuO and Cu_2O crystalline phases. The average size of the crystallites (D), index number, diffraction angles (2θ), full width at half maximum (FWHM) and the numbers of JCPDS cards used for the elucidation of the crystalline phases are compiled in Table 2. It is interesting to highlight that the peaks are broad, indicating a small size of the particles. It must be pointed out that the diffraction peak corresponding to amorphous carbon -commonly found at 25°- was not observed in the XRD patterns. This is a clear indicative that most of carbon atoms could be intercalated within the copper oxides networks, as also reported for C-doped TiO_2 photocatalysts [35].

Regarding optical features, the UV–vis diffuse reflectance spectrum of the catalyst (Fig. S4, SM) showed a profile with a marked reflectance decrease above 600 nm, ascribed to the band absorption edge of the nanocrystalline Cu_2O [25,26,41] This observation agrees with the formation of Cu_2O crystalline phase in the photocatalyst in agreement with the XRD pattern. An inflexion point was also observed at 575 nm in the diffuse reflectance spectrum, which is associated with the localized surface plasmon resonance due to the elemental Cu phases detected in the XRD as discussed above. On the other hand, the application of the Tauc equation to the diffuse reflectance data to estimate the optical bandgap rendered values of ca. 1.4–1.5 eV for the first optical feature and ca. 1.9–2.0 eV for the second one (Fig. S5, SM). Although these estimated band gap values agree with those reported in the literature for other copper oxide-based catalysts (e.g., 1.2–1.7 eV for CuO and 1.9–2.4 eV for Cu_2O) [25,26], they should be taken with care, as the application of Tauc equation is not recommended in materials with strong absorption features [42], as it is the case of herein studied Cu@C photocatalyst. Nevertheless, based on this data both copper oxide crystalline phases are considered the photoactive sites of the prepared Cu@C catalyst.

3.2. Tartrazine adsorption studies

Before performing the photocatalytic assays, the affinity of tartrazine towards the surface of Cu@C photocatalyst was investigated by equilibrium and kinetic adsorption studies at 20 °C under dark conditions and using a catalyst loading of 1 g L^{-1}. The adsorption kinetics (Fig. 3**a**) for different initial concentrations of the dye indicate that the uptake of the dye is rather fast, achieving the equilibrium uptake within 60–120 min. The equilibrium adsorption isotherm was recorded after 120 min (Fig. 3**b**) and showed a concave shape towards the abscissa with an incipient plateau at high equilibrium concentrations, corresponding to an L-type isotherm according to Giles classification [43].

This shape indicates that steady-state adsorption conditions are not fully achieved in the range of dye concentrations studied, but

Table 1
Summary of the proximate and EDS analysis of Cu@C catalyst.

Moisture[a] (wt%)	Inorganic content[a] (wt%)	Carbon content[a] (wt%)	C [b] (wt%)	O [b] (wt%)	Cu [b] (wt%)
1.6 ± 0.1	78.1 ± 0.5	20.3 ± 0.1	87.9 ± 0.9	4.7 ± 0.1	7.4 ± 0.1

[a] Proximate analysis; [b] Obtained from SEM-EDS analysis of the particles shown in **Fig. S2 (SM)**.

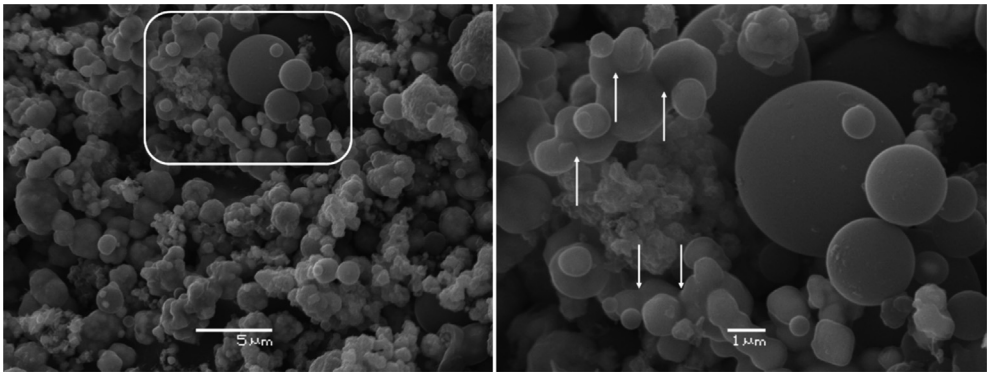

Fig. 1. SEM images of Cu@C catalyst.

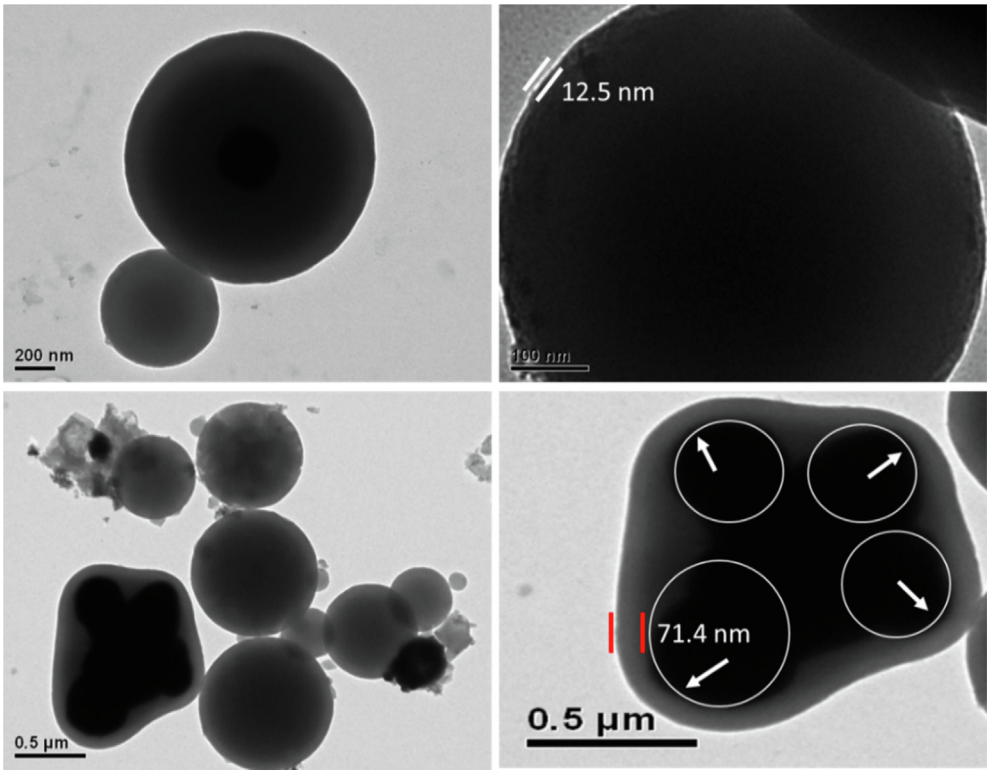

Fig. 2. Selected TEM images of Cu@C catalyst.

Table 2
Summary of selected textural parameters, surface pH, optical energy band gap, and main crystalline parameters of CuC of Cu@C catalyst.

S_{BET} (m^2/g) [a]	V_{total} (cm^3/g) [b]	V_{micro} (cm^3/g) [c]	Micropores(%) [d]	pH_{PZC}	E_{gap} (eV) [e]
90	0.07	0.04	48	5.3 ± 0.1	(*) 1.4–1.5 (**) 1.9–2.0

[a] BET specific surface area; [b] Total pore volume evaluated at $P/P_o \cong 0.99$; [c] Micropore volume evaluated from the Dubinin-Radushkevich equation [37]; [d] Fraction of micropores; [e] Optical energy band gap corresponding to the (*) first and (**) second optical features.

Crystalline phase	**Index Numbers**	**2θ[a]**	**FWHM (rad) [b]**	**D (nm) [c]**	**JCPDS Card**
Cu	(1 1 1)	43.29	0.0036	38	01–085-1326
CuO	(1 1 1)	38.69	0.0070	19	01–072-0629
Cu_2O	(1 1 1)	36.42	0.0059	23	05–0667

[a] Diffraction angles (2θ). [b] Full width at half maximum (FWHM). [c] Average size of crystallites (D) according to Eq. (1).

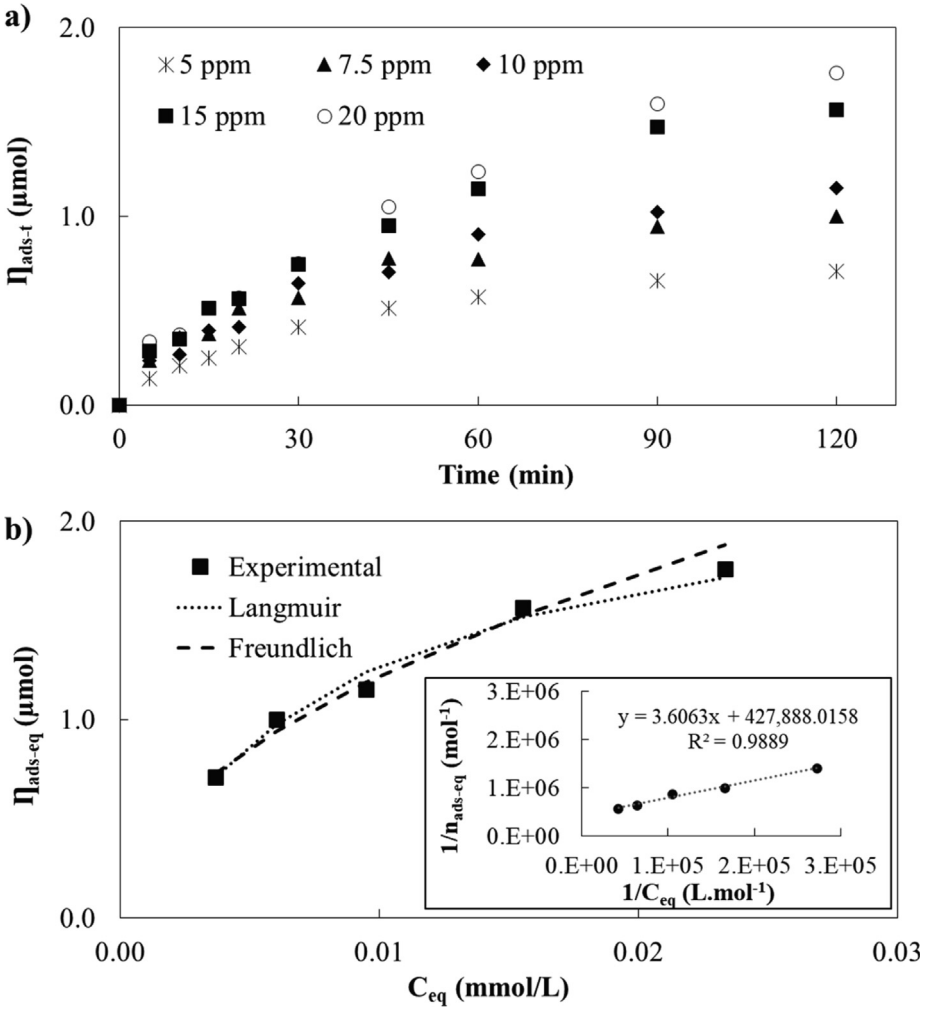

Fig. 3. a) Kinetics of Y5 adsorption in the dark for a Cu@C catalyst loading of 1 g·L^{-1}; b) Experimental equilibrium adsorption isotherm (symbols) and fitting to Langmuir and Freundlich models (lines). Inset: Linear regression according to Langmuir model.

rather a progressive filling of the adsorption sites takes place. The equilibrium adsorption isotherm data was best fitted to the Langmuir model, rendering a computed maximum adsorption capacity of ca. 2.3 µmol. This corresponds to a surface coverage varying from 75 to 43% for the highest and lowest initial concentrations, respectively. In addition, the remarkably high value of K_L obtained from the linear regression of Langmuir model (ca. 1.2 × 10^5 L·mol^{-1}) suggests an important chemical interaction between the dye and the catalyst's surface, despite its moderate specific surface area (90 m^2·g^{-1}, Table 2).

The relatively high coverage of the dye at the lowest initial concentration of 5 ppm suggests that the photocatalyst is expected to be efficient at such concentration. Hence, the optimization of the catalyst loading was limited to the lowest dye initial concentration. Furthermore, the photocatalytic assays in the CPC reactor will be carried out in realistic conditions of 2 ppm of the dye that corresponds to concentrations commonly found in real wastewaters from local food industries.

3.3. Photocatalytic performance under artificial solar light in a slurry batch reactor

3.3.1. Optimization of the catalyst loading.

As mentioned-above, the lowest dye initial concentration was used to investigate the effect of the catalyst loading. It is important to point out that at these conditions, the photolytic test of irradiation of the dye in the absence of the catalyst showed negligible changes in the concentration of the dye (Fig. S6, SM) after 5 h irradiation under artificial solar light. This confirms that the modifications in the concentration of the dye upon irradiation in the presence of the photocatalyst are exclusively ascribed to the photocatalytic degradation in heterogeneous phase.

The kinetic data of the photocatalytic assays was analyzed by the first- and second-order reaction-rate models. The half-order kinetic model (i.e., predominance of collisions among tartrazine molecules themselves) was discarded based on the negligible photolytic degradation of the dye in the absence of catalyst. Fig. 4**a** shows the kinetics of Y5 photodegradation as a function of time for different catalyst loadings. A summary of kinetic data corresponding to the dark adsorption and photodegradation reaction of the dye as a function of the catalyst loading is compiled in Table 3.

According to the linear regression factors obtained from the fitting of the experimental data to the different models (Table 3), the first-order reaction-rate model fitted much better than the second-order model. This is consistent with the abundant data from the literature, where photocatalytic experimental data at low concentration is commonly better described by a pseudo-first order kinetic model [44,45].

It is clear from the evolution of the concentration of tartrazine that the photocatalytic activity increased with the catalyst loading. For instance, conversions of 39% and 93% of Y5 were obtained after

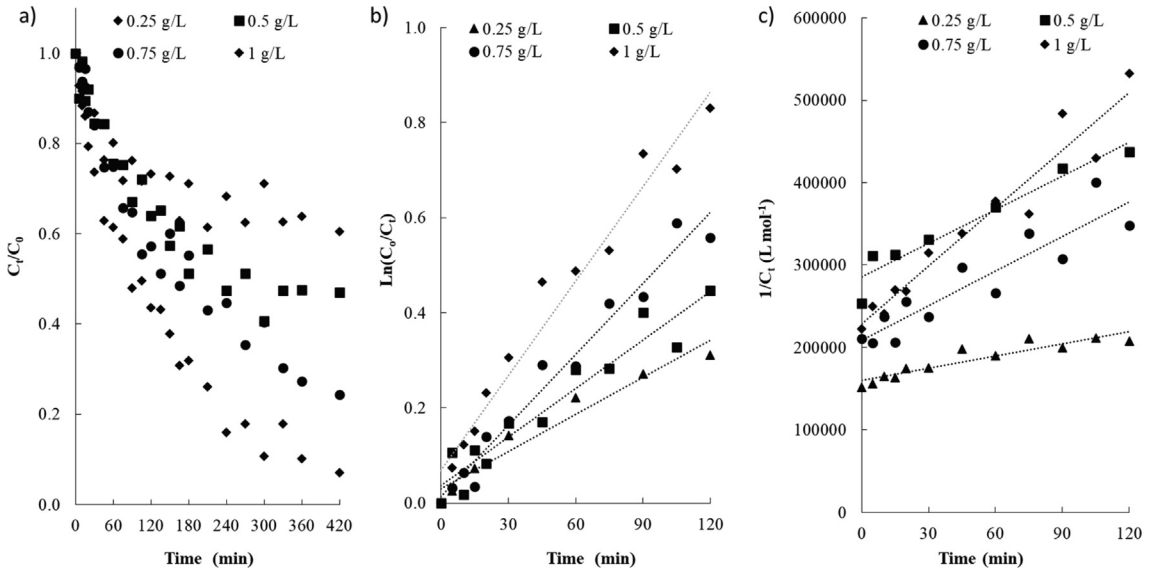

Fig. 4. a) Kinetics of Y5 photodegradation under artificial solar light at various Cu@C catalyst loadings for an initial concentration of 5 ppm of the dye (symbols); b) first-order, and c) second-order reaction-rate linear representation (lines) of the experimental data.

Table 3
Kinetic parameters for the dark adsorption and photocatalytic degradation of 5 ppm of Y5 as function of photocatalyst loading.

Loading ($g\ L^{-1}$)	η_{ads} ($\mu mol\ g^{-1}$) [a]	$k_{app} \times 10^{-3}$ (min^{-1}) [b]	R_1^2 [c]	$k_2 \times 10^{+2}$ ($L\ mol^{-1}\ min^{-1}$) [d]	R_2^2 [e]	n_{deg}(%) [f]
0.25	10.9 ± 0.2	2.6 ± 0.1	0.948	4.9 ± 0.7	0.856	39
0.50	6.0 ± 0.2	3.4 ± 0.3	0.922	13.6 ± 0.9	0.934	53
0.75	5.8 ± 0.2	5.0 ± 0.2	0.970	14.0 ± 2.2	0.841	76
1.0	5.0 ± 0.1	6.6 ± 0.2	0.966	23.4 ± 0.9	0.937	93

[a]Y5 adsorption in the dark after 60 min; [b] First-order apparent rate-constant obtained from the linear regression: $Ln(C_o/C_t) = k_{app} \cdot t$; [c] Quadratic factor obtained from the treatment of the kinetic data of degradation according to a 1st-order reaction-rate; [d] 2nd-order apparent rate-constant obtained from the linear regression: $(1/[C_t]) = [(1/[C_{Eq}] + k_2 t]$; [e] Quadratic factor obtained from the treatment of the kinetic data of degradation according to a second-order reaction-rate; [f] Y5 conversion after 420 min irradiation defined as $n_{deg} = [1 - (C_t/C_o)] \cdot 100$.

7 h of irradiation for loadings of 0.25 g L^{-1} and 1 g L^{-1}, respectively. Such increase in the photoactivity must be associated to the high density of catalytic active sites when high loadings are used.

As seen in Table 3, the amount of dye adsorbed decreased with the catalyst loading, spanning from 10.9 μmol g^{-1} for the lowest (0.25 g L^{-1}) to 5.0 μmol g^{-1} for the highest catalyst loading (1 g L^{-1}). This fall in the uptake does not follow a linear trend, since the amount adsorbed at the highest loading is about 1.9 times higher than that of the lowest loading –despite a 4-times increase in the amount of catalyst–. This is in line with the saturation of the adsorption above-mentioned at high loadings, which can be most likely attributed to the low surface area of the photocatalyst (Table 2).

On the other hand, the conversion of the dye after 7 h of irradiation followed a clear decreasing and monotonic trend for catalyst loadings above 0.50 g L^{-1}; this may be indicative of a saturation of the adsorption sites, most likely due a multiple fragmentation of Y5 molecules during the photocatalytic reaction [29].

The first-order apparent rate-constants (k_{app}) were estimated as the best kinetic parameter to compare the photoactivity (Fig. 4**b**). Table 3 shows that k_{app} increased with the catalysts loading (e.g., from 2.6 × 10^{-3} min^{-1} to 6.6 × 10^{-3} min^{-1}, for 0.25 and 1 g L^{-1}, respectively). In other words, a decrease of ca. 2.2 times in the adsorption capacity of the system (driven by a higher catalyst loading) had a positive influence on the photoactivity, by a factor of ca. 2.6 times higher. Based on the obtained data, the optimal catalyst loading for the photocatalytic reaction carried out in a slurry photoreactor with artificial solar light can be settled to 1 g L^{-1}. However, such high catalyst loading is not adequate for its application in a CPC photoreactor due to operating problems related to the deposition of the catalyst during the operation (thus, inhomogeneous irradiation of the photocatalyst particles) and the high light scattering [30]. For these reasons, a photocatalyst loading of 0.25 g L^{-1} was selected for the degradation assays carried out in the CPC reactor under outdoor solar irradiation.

3.3.2. *Effect of the initial concentration of Y5*

Using a nominal catalyst loading (1 g L^{-1}), the effect of the initial concentration of the dye on the photocatalytic conversion was investigated in the range of 5–15 ppm. A similar experimental protocol was used for all the assays, with an initial step of dark adsorption followed by the light exposure using artificial solar light. As above-mentioned, kinetic data was fitted to the first- and the second-order kinetic models. Fig. 5**a** shows the kinetics of Y5 conversion as a function of the initial concentration of the dye. A summary of the main kinetic parameters corresponding to the adsorption and photodegradation steps of Y5 after 7 h of irradiation is compiled in Table 4.

As already observed for the effect of the catalyst loading, a better fitting was obtained for the first-order reaction-rate model, suggesting that different types of active sites can be present in the material. This will be later discussed below based on the photocatalytic tests performed in the presence of radical scavengers. As seen, the amount of tartrazine adsorbed increased from ca. 5.0 to 11.1 μmol g^{-1} when the initial concentration increased from 5

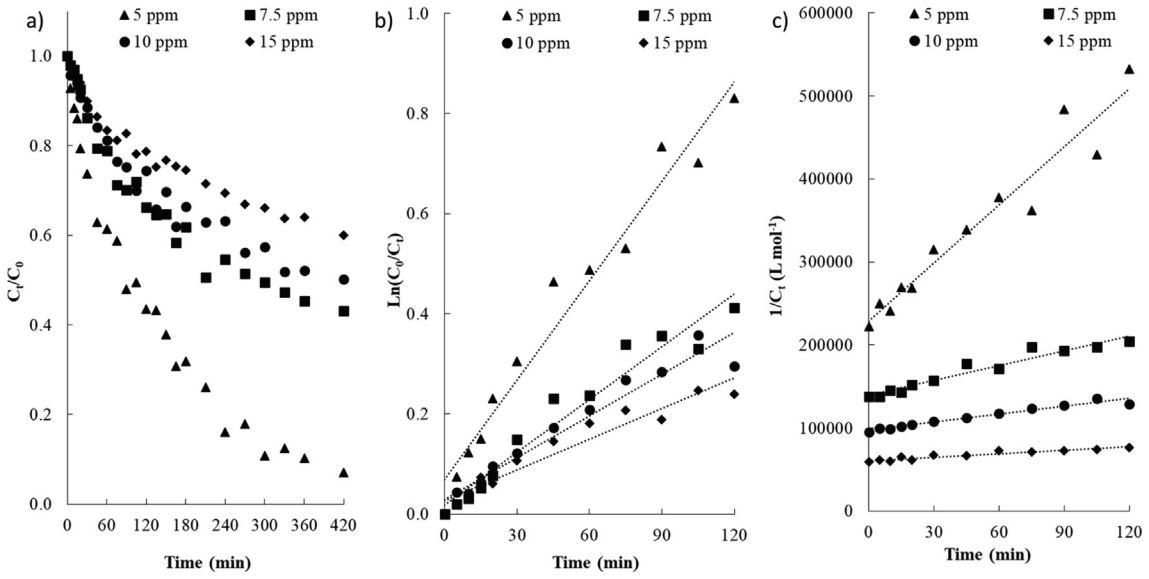

Fig. 5. a) Kinetics of Y5 photodegradation under artificial solar degradation for a catalyst loading of 1 g L^{-1} and varied initial concentrations (symbols); b) first-order, and c) second-order linear fitting (lines) of the kinetic data.

Table 4
Kinetic parameters of adsorption and degradation of Y5 as a function of the initial concentration of Y5 at constant loading (1 g L^{-1}).

Initial Concentration (ppm)	η_{ads} (μmol g^{-1}) [a]	$k_{app} \times 10^{-3}$ (min^{-1}) [b]	R^2 [c]	$k_2 \times 10^{+2}$ (L mol^{-1} min^{-1}) [d]	R_2^2 [e]	n_{deg}(%) [f]
5	5.0 ± 0.1	6.6 ± 0.2	0.966	23.4 ± 0.9	0.937	93
7.5	6.8 ± 0.1	3.5 ± 0.1	0.947	5.95 ± 0.4	0.939	57
10	8.2 ± 0.2	2.8 ± 0.1	0.944	3.18 ± 0.1	0.955	50
15	11.1 ± 0.2	2.1 ± 0.1	0.930	1.40 ± 01	0.912	40

[a]Y5 adsorption in the dark after 60 min; [b] First-order apparent rate-constant obtained from the linear regression: $Ln(C_o/C_t) = k_{app} \cdot t$; [c] Quadratic factor obtained from the treatment of the kinetic data of degradation according to a first-order reaction-rate; [d] Second-order apparent rate-constant obtained from the linear regression: $(1/[C_t]) = [(1/[C_{Eq}] + k_2.t]$; [e] Quadratic factor obtained from the treatment of the kinetic data of degradation according to a second-order reaction-rate; [f] Y5 conversion after 420 min irradiation defined as $n_{deg} = [1 - (C_t/C_o)].100$.

to 15 ppm; this points out to a gradual coverage of the surface of the catalyst at high concentrations, as mentioned above.

Regarding the photocatalytic activity, the degradation of the dye after 7 h of irradiation was higher (ca. 93% disappearance) for 5 ppm of initial concentration, compared to 40% when the reaction is carried out from a solution of 15 ppm of the dye (Table 4). This is somewhat expected since the amount of dye increases but the number of photons is similar. However, it is interesting to point out that the first-order apparent rate constant (k_{app}) decreased by 3 times (Table 4) as the concentration of Y5 increased from 5 to 15 ppm. This indicates that the rate of degradation of the dye is faster at low concentrations, despite the number of molecules in the vicinity of the catalytic active sites is lower (i.e., lower amount adsorbed at 5 ppm). Such behavior may be attributed to a competitive simultaneous degradation of the intermediates created upon the cleavage of Y5, as reported in a previous work [29]. Other researchers obtained similar results [46] and suggested that at high initial concentrations of Y5, a decrease in the number of active sites can remarkably affect the production of hydroxyl (·OH) and superoxo anion ($O_2^{\cdot -}$) radicals, thereby reducing the reaction efficiency.

3.4. Photodegradation of Y5 under natural solar irradiation using a CPC photoreactor.

Based on the optimization studies, the operating conditions for the degradation assays carried out in the CPC reactor under outdoor natural solar irradiation were settled at a dye initial concentration of 2 ppm (representative of the concentrations commonly found in wastewater in the food industry for this azo-dye) and a photocatalyst loading of 0.25 g L^{-1}. The latter was chosen to avoid issues of particles deposition and a deficient and non-homogeneous irradiation of the catalysts due to a large contribution of light scattering of the catalyst particles [30]. Fig. 6a shows the kinetics of the photocatalytic degradation of Y5 in the pilot CPC photoreactor as function of the experimental time (see experimental section) [34]. Fig. 6**b** shows the linear regression of the kinetic data**.** The results are compared with those obtained at the same experimental conditions in a slurry reactor using artificial solar light.

As already observed for the irradiation under artificial solar light (Fig. S8, SM), the photolysis of 2 ppm of tartrazine was negligible when using the CPC photoreactor under natural sunlight (Fig. S7, SM). In addition, the amount of dye adsorbed in the dark was independent of the type of photoreactor, with values of ca. 15% and ca. 17% after 60 min in both cases (Table 5). This is important as it allows to attributing any likely differences in the performance to the photocatalytic reaction itself, rather than to the adsorption step.

As seen, the kinetic data of the photocatalytic degradation of yellow 5 in the CPC photoreactor under natural solar light fitted much better to the first-order kinetic model. On the contrary, the second-order kinetic model fitted better when the reaction was carried out in the slurry photoreactor under artificial solar light. This suggests that at high irradiation fluxes provided by the artificial solar light, the catalytic reaction does not only depend on the concentration of the dye, but also on that of other reactants (likely

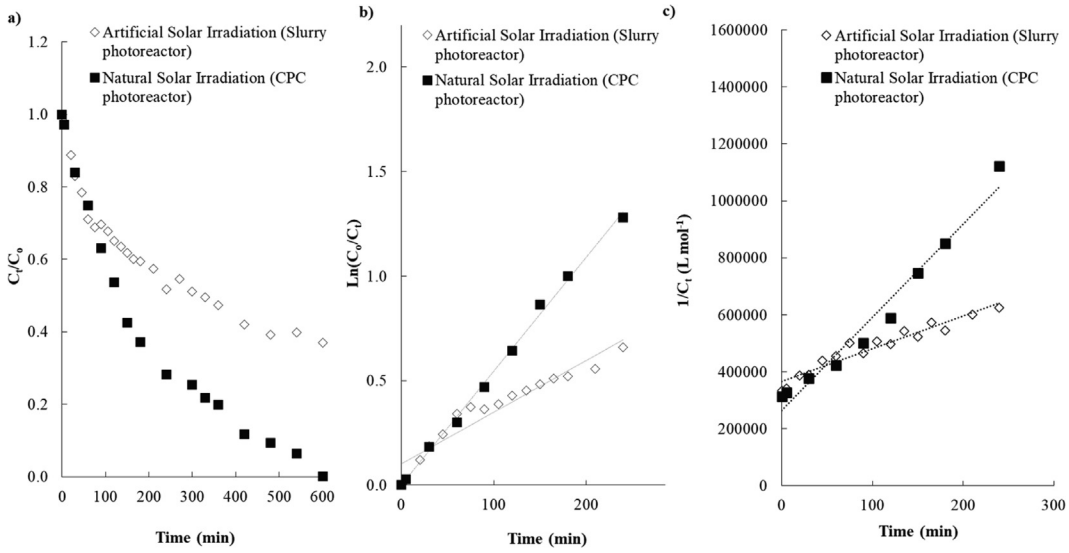

Fig. 6. Comparison of the photocatalytic activity of Cu@C catalyst under artificial and natural solar light using two photoreactor configurations: a CPC photoreactor and a slurry photoreactor. Catalyst loading was fixed to 0.25 g L^{-1} and initial concentration of the dye to 2 ppm; a) Kinetics of Y5 concentration in the photocatalytic assays (symbols); b) First-order, and c) Second-order linear fitting (lines) of the kinetic data.

Table 5
Summary of adsorption in the dark and kinetic parameters of the photocatalytic degradation of Y5 using artificial UV–vis and natural solar irradiation. Initial concentration 2 ppm and 0.25 g L^{-1} catalyst loading.

Type of Irradiation	η_{ads} (μmol g^{-1}) [a]	$k_{app} \times 10^{-3}$ (min^{-1}) [b]	R_1^2 [c]	$k_2 \times 10^{+2}$ (L mol^{-1} min^{-1}) [d]	R_2^2 [e]	n_{deg}(%) [f]
Natural solar irradiation	15.3 ± 0.3	5.5 ± 0.1	0.997	32.7 ± 0.9	0.968	100
Artificial irradiation	16.6 ± 0.5	2.5 ± 0.2	0.916	11.4 ± 0.8	0.932	63

[a] Y5 adsorption in the dark after 60 min; [b] First-order apparent rate-constant obtained from the linear regression: $Ln(C_o/C_t) = k_{app} \cdot t$; [c] Quadratic factor obtained from the treatment of the kinetic data of degradation according to a 1st-order reaction-rate; [d] 2nd-order apparent rate-constant obtained from the linear regression: $(1/[C_t]) = [(1/[C_{Eq}] + k_2.t]$; [e] Quadratic factor obtained from the treatment of the kinetic data of degradation according to a second-order reaction-rate; [f] Y5 conversion after 420 min irradiation defined by $n_{deg} = [1 - (C_t/C_o)].100$.

the degradation intermediates). It also indicates that at high photon fluxes intramolecular reactions between tartrazine molecules and some intermediate products would take place; under these conditions, enough energy is supplied to overcome the activation barrier of these type of reactions.

It can be seen in Fig. 6**a** that Y5 completely disappeared after 600 min of exposure to natural solar light, compared to 60% conversion using artificial solar light. In addition, the reaction rate is slower for the latter configuration (Table 5), indicating that Cu@C catalyst is ca. 2.2 times more efficient (in terms of reaction rate) when exposed to natural solar light. This is attributed to the large differences in the photon flux in both configurations, being significantly higher for the artificial solar light (ca. 1950 W m^{-2}) than in the CPC using natural solar light (ca. average 886 W m^{-2}, ranging from 664 to 1018 W m^{-2}). In this regard, it has been experimentally shown [11,13,30] that above a certain photon flux, the reaction rate may change due to the excess of photogenerated species. In consequence, the quantum yield of the photocatalytic reaction decreases due to a high recombination rate of the e^-/ h^+ pairs formed. It has also been reported that the external mass transfer of pollutant from the bulk solution to the adsorption sites can limit the photocatalytic rate at high irradiation intensities [47]. In our study, based on the similar uptake observed for both configurations and since the adsorption step is carried out before the exposure to light, we can assume that the mass transfer of the dye towards the surface of the photocatalyst does not affect (or affects equally) the catalytic performance. Thus, the high efficiency of Cu@C catalyst under natural solar light in the CPC photoreactor (compared to the slurry reactor and artificial light) points out to a better performance under moderate photon fluxes, where the surface recombination is minimized [48].

To verify this, the kinetics of disappearance of Y5 is shown in Fig. 7**a** in terms of the instantaneous solar exposure (t_R. Φ, min W·m^{-2}), calculated as the product of the residence time (t_R) (see experimental section) and the photon flux (Φ) expressed in W·m^{-2}. The difference observed in both configurations point out that the solar exposure is a relevant parameter in the reaction rate of the photodegradation of tartrazine.

As seen, for a similar solar exposure of ca. 2.7x10^5 min W·m^{-2}, conversions of 100% and 40% were obtained for the CPC and the slurry reactor, respectively. This large difference is attributed to the excess of irradiation under the latter configuration, which would be responsible for a higher recombination rate (thus lower photocatalytic performance). Similar findings pointing out a better performance of TiO_2 for the degradation of tartrazine under natural solar exposure have been reported by Chekir and co-workers [48]. In this case, the authors reported the 99% conversion of a 10 ppm solution of the dye after 300 min using natural solar light, compared to 30% conversion using artificial UV irradiation.

It should be pointed out that CPC photoreactors do not concentrate photons within the tubes, as opposed to solar concentrators for solar thermal energy [11,13,30,40]; thus the temperature of the reaction does not increase during the irradiation. In our study, for the series of experiments carried out in the CPC photoreactor, the temperature varied from 12 to 18 °C at the beginning of the catalytic assay, to 14–20 °C after 6 h of irradiation. In the case of

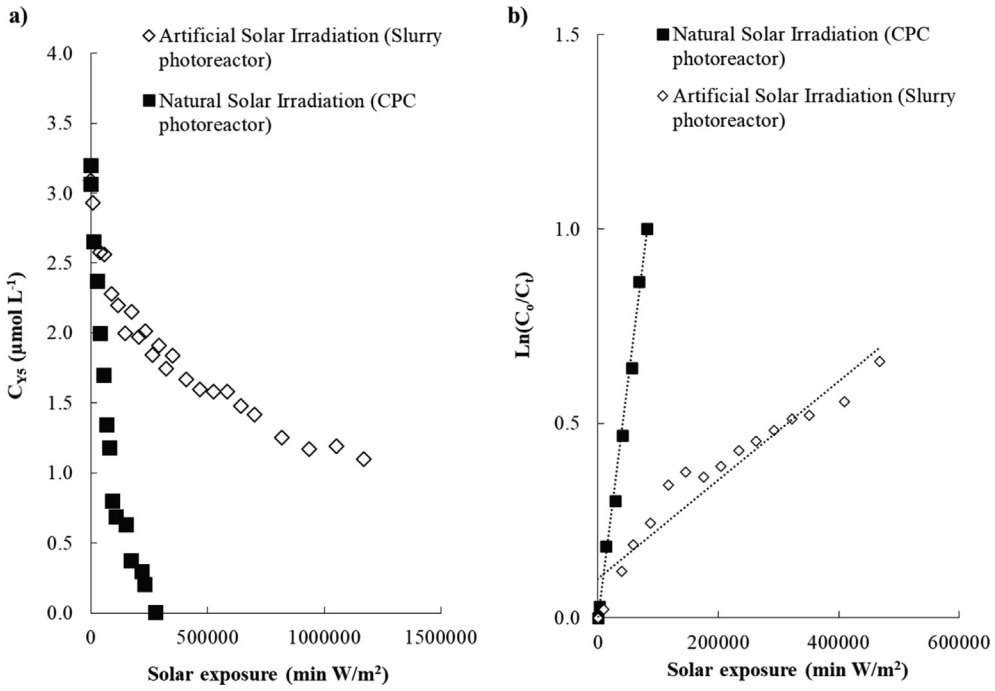

Fig. 7. a) Kinetic disappearance of Y5 on Cu@C catalyst as a function of the solar exposure (min·W·m^{-2}) under natural solar irradiation and artificial solar light (symbols); b) first-order linear fitting of the kinetic data (lines).

the slurry reactor under artificial solar light, the increase in the temperature was of ca. 4 °C (from 25 °C up to 29 °C). Thus, degradation of the dye due to thermo(photo)catalytic reactions arising from the irradiation of the dark carbon and/or copper matrices (localized resonance plasmon) can be disregarded in both configurations.

The evolution of the degradation reaction was also followed by the determination of the total carbon content (TC). Fig. 8 shows the TC evolution as a function of the irradiation type for both photoreactors. The initial TC value of 0.64 ppm is in agreement with the expected value corresponding to 0.61–0.60 ppm, accounting for the initial concentration (ca. 2 ppm of azo-dye corresponding to 0.72 ppm of TC) after subtracting the fraction adsorbed of ca. 15% and 17% for batch and CPC photoreactor.

The TC decreased when the degradation was performed under natural solar irradiation in the CPC photoreactor, achieving a final TC value of 0.19 ppm (ca.70% decrease), confirming a high extent of mineralization of the dye. In contrast, the values of TC increased up to 3.5 ppm after 600 min irradiation when artificial solar light was used. We attribute this behavior to a partial decomposition of the catalyst (likely releasing carbon-based groups to the solution) due to the high photon flux of the artificial solar light (1950 W m^{-2}). Thus, the lower photoactivity may also be ascribed to these modifications of the catalyst (e.g., loss of adsorption/photoactive sites).

3.5. Investigation of the mechanism

To investigate the mechanism of the photodegradation of the dye in both photoreactor configurations, additional photocatalytic assays were carried out in the presence of benzoquinone and isopropyl alcohol as scavengers of superoxide radical ($\cdot O_2^-$) and hydroxyl radical (·OH), respectively. Fig. 9 shows that in the presence of

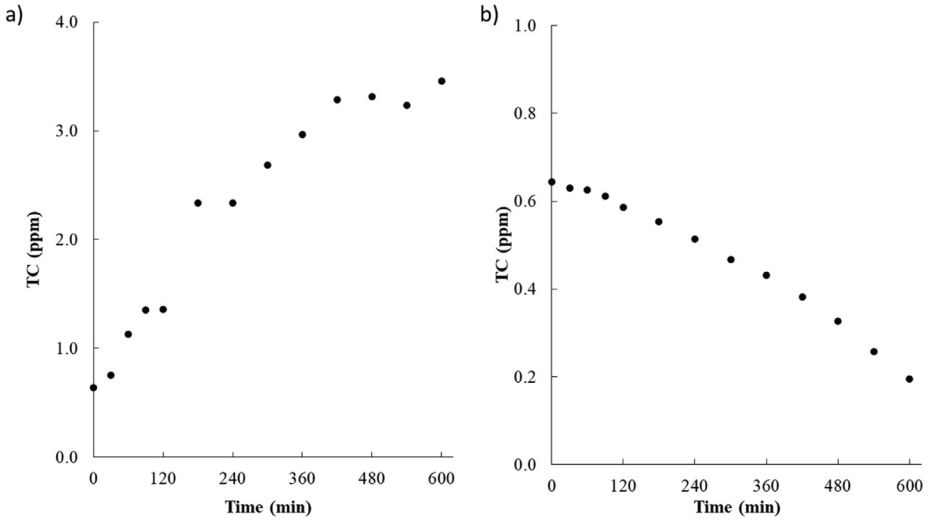

Fig. 8. Total carbon (TC) evolution detected during the photodegradation of yellow 5 on irradiated Cu@C photocatalyst: a) artificial solar light; b) natural solar light. Experimental conditions: 2 ppm Y5 and 0. 25 g L^{-1} catalyst loading.

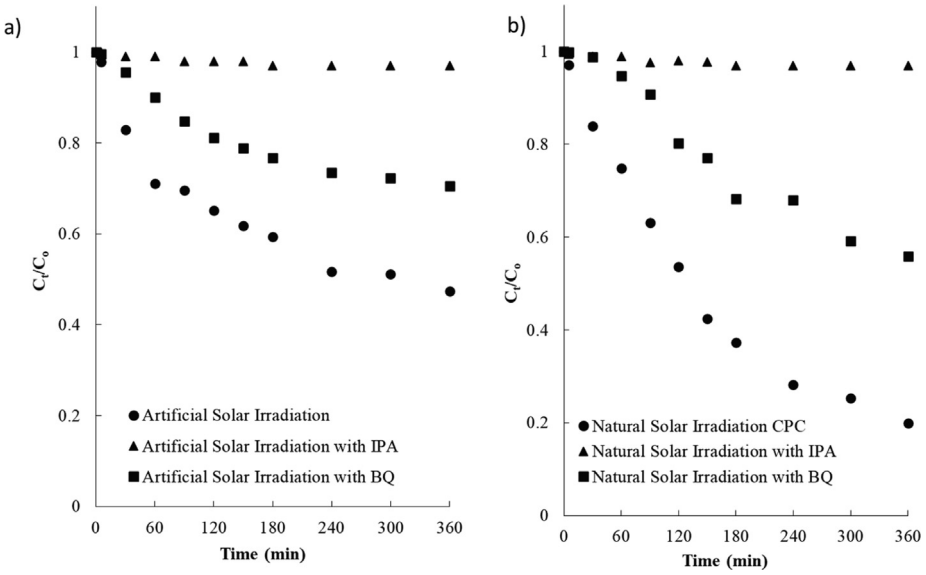

Fig. 9. Kinetics of Y5 photodegradation on Cu@C photocatalyst in the absence and presence of IPA and BQ scavengers: a) Artificial solar light; b) natural solar light.

IPA as scavenger of hydroxyl radicals, the disappearance of the dye was practically negligible for both photoreactors (ca. 3% after 6 h irradiation, compared to 53% and 80% in the absence of the scavenger after 6 h of artificial and natural solar light). In contrast, the trapping of superoxide radicals had a moderate influence on the kinetics of degradation of the azo-dye, with conversions of 29% and 54%.

Therefore, it seems logical to suggest that two different types of active sites are involved in this reaction. This would be in agreement with the optical features observed for the Cu@C catalyst as discussed above; thus, both metallic active sites and Lewis's acid sites such as elemental Cu and Cu oxides, could be associated with the mechanisms of reaction. Hence, at low catalyst loading and low initial concentration of yellow 5, the photocatalytic degradation would proceed via the simultaneous i) unimolecular electrophilic (E_1) addition of the superoxide radical ($\cdot O_2^-$) to the dye and ii) the unimolecular substitutional nucleophile (SN_1) attack by hydroxyl radicals ($\cdot OH$).

Based on the results of the scavenger tests we propose a photocatalytic degradation pathway dominated by the cleavage of the N=N azo bond by successive attacks of $\cdot OH$ [29,49-51], as shown in Fig. 10.

This mechanism agrees with other studies reported in the literature based on experimental and computational methods [47-51], proposing the nucleophilic attack of the N=N bond as the initial step. Popadić et al. [49] and Ali et al. [50] also reported that the catalytic degradation of tartrazine follows different pathways as a function of the pH of solution, including the attack of •OH radicals at slight acidic pH. This is in agreement with our results, since the photocatalytic assays have been carried out at pH 5.

It is interesting to highlight the degradation mechanism has been discussed based on the performance of the photocatalyst in the presence of scavengers and compared to previous reports in the literature. Regarding the role of the carbon matrix, in our experimental conditions of low contribution of UV photons, the contribution of the carbon phase to the photocatalytic activity is

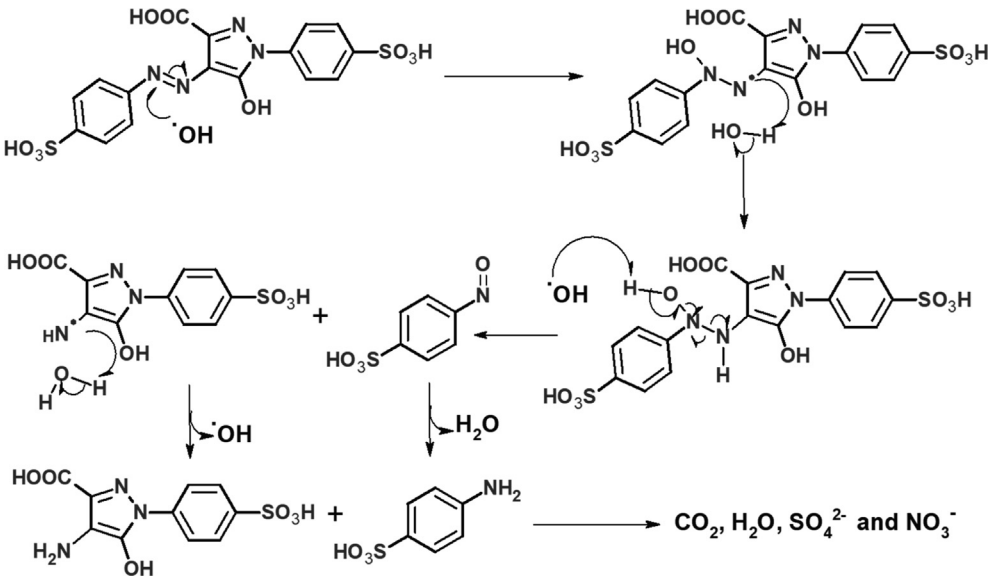

Fig. 10. Proposed mechanism for the Y5 degradation under natural solar irradiation. (Adapted from the mechanism reported in reference [29]).

not expected to be high. Thus, the carbon matrix would be mostly acting as a protective layer to absorb the high energy photons, preventing the lixiviation of the copper-species.

3.6. Lixiviation tests

The catalyst based on CuO in the absence of the carbon matrix was prepared and did not show photocatalytic activity for the degradation of the dye under simulated solar light. We believe this is attributed to the instability of the prepared materials under high photon fluxes, since copper lixiviation was detected when the protective layer of the carbon matrix is not present. Thus, the following discussion is referred to Cu@C catalyst.

Fig. 11 shows the evolution of Cu ions in solution for the two types of photoreactors. It can be seen that the leaching of copper is negligible, since the obtained values were lower than 0.05% and 0.01% Cu for artificial and natural solar light, respectively.

Even though, a higher value of Cu was detected when a high photon flux was used (artificial irradiation); this could be associated to a gradual degradation of the protective carbon layer of the catalysts under these conditions, as evidenced by the results of total carbon content shown in Fig. 8**a**. Furthermore, it can be concluded no lixiviation of copper species was detected in solution confirming the stability of the photocatalyst when CPC photoreactor is used. In summary, herein obtained values for the degradation of tartrazine degradation using a Cu@C catalyst under artificial or natural solar irradiation are in the same order or even are higher than the values recently reported for alternative catalysts such as Fe_2O_3/Mn_2O_3 composites [52], Zn_2SnO_4-V_2O_5 nanocomposite [53], two-dimensional Zn-Co [54] catalyst, Ag_2CO_3-loaded S-doped graphene oxide [55], TiO_2 immobilized on membranes [56], and Cu-based catalysts [46,48-58], including $CeO_2/CuO/Ag_2CrO_4$ ternary heterostructures based on CeO_2/CuO [58], and Cu/CuO nanorods under visible LED light irradiation. However, most of this literature did not mention or include quantitative lixiviation studies of Cu-based active phase as in the present work.

In conclusion, since Cu@C is a low-cost and biocompatible catalyst, we do believe this material is a potential alternative to be used for the photodegradation of food industry azo-dyes. It is clear from results discussed above that Cu@C material is an efficient photocatalyst under outdoor natural solar conditions. The experiments were carried out for a total of 10 h of irradiation during consecutive days; this is similar than the total irradiation time reported in the literature for most photocatalytic tests after several cycles (ca. usually of 2–3 h per cycle). The present Cu@C photocatalyst is currently being tested in weekly photocatalytic assays in the CPC photoreactor for over one year now, aiming to evaluate the performance along different seasons of the year (at varied photon fluxes and outdoor temperatures) to validate the efficiency of Cu@C photocatalyst under real climatic conditions.

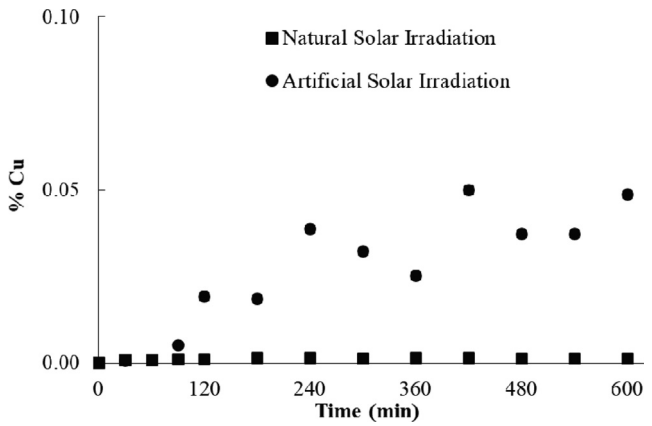

Fig. 11. Copper lixiviation under artificial and natural solar irradiation.

4. Conclusions

An efficient C-containing Cu-based photocatalyst has been prepared and used in the degradation of yellow 5 dye in two configurations: a slurry photoreactor under artificial solar light and a composed parabolic collector (CPC) photoreactor under natural solar light. A good photocatalytic performance was obtained for the catalyst, compared to other alternative metallic semiconductors reported in the literature. Such performance is ascribed to the combination of a good affinity between the dye and the photocatalyst surface, combined with various copper-based species with photoactivity under visible light. The optimization of key operating parameters for the photocatalytic reaction in the slurry reactor under artificial solar light indicated an enhanced performance at low initial concentrations of the dye and low catalyst loadings. Under these experimental conditions, the catalyst showed a better photocatalytic performance using a CPC photoreactor upon natural solar light irradiation at a moderate photon flux. Data has shown that the photon flux is an important factor to be considered in the photodegradation process of Y5; the strong irradiation conditions of the solar simulator compared to the natural light in the CPC rendered a poor catalytic performance, likely due to an increased recombination of charge carriers and to the degradation of the catalysts under severe irradiation conditions.

The catalytic tests carried out in the presence of scavengers of reactive oxygen species confirmed that the degradation of the dye proceeded mainly through the nucleophilic attack of ·OH radicals to the azo bond. No evidences for photothermal effects or photolytic bleaching of the dye were observed. Furthermore, although the photocatalyst suffered some modifications when exposed to high photon fluxes (artificial solar light), it was stable under natural solar irradiation in the continuous-flow photoreactor. This is attributed to the protector role of the carbon matrix preventing the lixiviation of the copper species to the solution.

Overall, it may be inferred that the prepared Cu@C photocatalyst is an economically sustainable, locally available, and efficient material to be applied for the removal of Y5 dye from effluents by adsorption and heterogeneous photocatalysis under natural solar irradiation. It is notably more efficient under natural sunlight, with a faster apparent rate constant compared to the slurry photoreactor configuration using a solar simulator. This is most important since most of the photocatalytic tests designed to evaluate the activity of novel materials are typically carried out under simulated solar light and disregard the effect of the photon flux on the performance of the material under real outdoor illumination conditions (natural solar light).

Declaration of Competing Interest

The authors declare that they have no known competing financial interests or personal relationships that could have appeared to influence the work reported in this paper.

Acknowledgments and Fundings

This research is ascribed within the cooperation framework between CNRS and Autonomous University of Chile. The authors thank the financial support of the Franco-Chilean network BIOCval2E (REDES-170004 project). P. Muñoz thanks to ANID-PIA/APOYO CCTE AFB170007 and ANID-FONDECYT 1190591 projects for the fellowships given during the PhD studies. P.S. Poon thanks

to ANID-PIA/APOYO CCTE AFB170007 project. J. Matos acknowledges the funds from Chilean projects: ANID-FONDEF ID19I10003; ANID-FONDEF ID15I20321; ANID-FONDECYT 1190591.

Ethical declaration

All the authors have read and approved to publish the paper in the Journal of Colloid and Interface Science journal. Authors declare the paper has not been published previously nor is it being considered by any other peer-reviewed journal.

Authorś contributions

P. Muñoz-Flores contributed to the synthesis, draft, and analysis of data. C.O. Ania contributed to characterization of the samples, data interpretation and writing the paper. P.S. Poon contributed with characterization of materials and analysis of results. J. Matos conceived and designed the manuscript, contributed to data analysis and interpretation, writing the paper, and assembled the contributions of all the authors.

Appendix A. Supplementary material

Supplementary data to this article can be found online at https://doi.org/10.1016/j.jcis.2022.05.042.

References

[1] N.F. Gray, Drinking Water Quality: Problems and solutions, second ed., Cambridge University Press, 2008.
[2] B. Jimenez-Cisneros, J.B. Rose (Eds.), Urban Water Security: Managing Risk, CRC Press, Taylor and Francis Group, UNESCO-IHP, 2009.
[3] C.P. Amézquita-Marroquín, P. Torres-Lozada, L. Giraldo, P.D. Húmpola, E. Rivero, P.S. Poon, et al., Sustainable production of nanoporous carbons: Kinetics and equilibrium studies in the removal of atrazine, J. Coll. Inter. Sci. 562 (2020) 252–267.
[4] https://es.unesco.org/themes/water-security/wwap/wwdr/2020, Taken 10 April 2022.
[5] P.R. Gogate, A.B. Pandit, A Review of imperative technologies for wastewater treatment I: Oxidation technologies at ambient conditions, Adv. Environ. Res. 8 (2004) 501–551.
[6] I.K. Konstantinou, T.A. Albanis, TiO_2-assisted photocatalytic degradation of azo dyes in aqueous solution: kinetic and mechanistic investigations: A review, Appl. Catal. B: Environ. 49 (2004) 1–14.
[7] M. Pera-Titus, V. Garcia-Molina, M.A. Banos, J. Giménez, S. Esplugas, Degradation of chlorophenols by means of advanced oxidation processes: A general review, Appl. Catal. B: Environ. 47 (2004) 219–256.
[8] M. Schiavello (Ed.), Photocatalysis and Environment: Trends and applications. NATO Science Series C, Springer, 1998.
[9] D.M. Blake, Bibliography of work on the photocatalytic removal of hazardous compounds from water and air, National Renewable Energy Laboratory, NREL/TP-510-31319. (November 2001).
[10] J. Gomes, J. Lincho, E. Domingues, R.M. Quinta-Ferreira, R.C. Martins, N-TiO_2 photocatalysts: A review of their characteristics and capacity for emerging contaminants removal, Water 11 (2019) 373.
[11] S. Malato, M.I. Maldonado, P. Fernández-Ibáñez, I. Oller, I. Polo, R. Sánchez-Moreno, Decontamination and disinfection of water by solar photocatalysis: The pilot plants of the Plataforma Solar de Almeria, Mater. Sci. Semiconductor Proc. 42 (2016) 15–23.
[12] I. Muñoz, J. Rieradevall, F. Torrades, J. Peral, X. Domènech, Environmental assessment of different solar driven advanced oxidation processes, Sol. Energy 79 (2005) 369–375.
[13] D. Robert, S. Malato, Solar photocatalysis: a clean process for water detoxification, Sci. Total Environ. 291 (2002) 85–97.
[14] K. Hashimoto, H. Irie, A. Fujishima, TiO_2 photocatalysis: a historical overview and future prospects, Jpn. J. Appl. Phys. 44 (2005) 8269–8285.
[15] L.F. Velasco, I.M. Fonseca, J.B. Parra, J.C. Lima, C.O. Ania, Photochemical behavior of activated carbons under UV irradiation, Carbon 50 (2012) 249–258.
[16] A. Fernández, G. Lassaletta, V.M. Jiménez, A. Justo, A.R. González- Elipe, J.M. Herrmann, et al., Preparation and characterization of TiO_2 photocatalysts supported on various rigid supports (glass, quartz and stainless steel). Comparative studies of photocatalytic activity in water purification, Appl. Catal. B. Envrion. 7 (1995) 49–63.
[17] J. Fenoll, E. Ruiz, P. Hellín, P. Flores, S. Navarro, Heterogeneous photocatalytic oxidation of cyprodinil and fludioxonil in leaching water under solar irradiation, Chemosphere 85 (2011) 1262–1268.
[18] S.Y. Kim, C.H. Ahn, J.H. Lee, Y.H. Kwon, S. Hwang, J.Y. Lee, et al., p-Channel oxide thin film transistors using solution-processed copper oxide, Appl. Mater. Interfaces 5 (2013) 2417–2421.
[19] D. Gao, J. Zhang, J. Zhu, J. Qui, Z. Zhang, W. Sui, et al., Vacancy- mediated magnetism in pure copper oxide nanoparticles, Nanoscale Res. Lett. 5 (2010) 769–772.
[20] V.D. Patake, S.S. Joshi, C.D. Lokhande, O.S. Joo, Electrodeposited porous and amorphous copper oxide film for application in supercapacitor, J. Mater. Chem. Phys. 114 (2009) 6–9.
[21] X. Zhang, J. Song, J. Jiao, X. Mei, Preparation and photocatalytic activity of cuprous oxide, Solid State Sci. 12 (2010) 1215–1219.
[22] X. Li, Y. Wang, Y. Lei, Z. Gu, Highly sensitive H_2S sensor based on template-synthesized CuO nanowires, RSC Adv. 2 (2015) 2302–2307.
[23] T.J. Richardson, J.L. Slack, M.D. Rubin, Electrochromism in copper oxide thin films, Electrochim. Acta 46 (2001) 2281–2284.
[24] M. Nolan, S.D. Elliot, Tuning the transparency of Cu_2O with substitutional cation doping, Chem. Mater. 20 (2008) 5522–5531.
[25] D. Tahir, S. Tougaard, Electronic and optical properties of Cu, CuO and Cu_2O studied by electron spectroscopy, Phys. Condens. Matter. 24 (2012) 175002.
[26] V. Niveditha, M.J.J. Fatima, S. Sindhu, Comprehensive interfacial study of potentio-dynamically synthesized copper oxide thin films for photoelectrochemical applications, J. Electrochem. Soc. 163 (2016) 426–433.
[27] A.Y. Kozlov, M.V. Dorogov, N.V. Chirkunova, I.M. Sosnin, A.A. Vikarchuk, A.E. Romanov, CuO nanowhiskers-based photocatalysts for wastewater treatment, Nano Hybrids and Composites 3 (2017) 183–189.
[28] M.A. Andrade, R.J. Carmona, A.S. Mestre, J. Matos, A.P. Carvalho, C.O. Ania, Visible light driven photooxidation of phenol on TiO_2/Cu-loaded carbon catalysts, Carbon 76 (2014) 183–192.
[29] P. Muñoz-Flores, P.S. Poon, C. Sepulveda, C.O. Ania, J. Matos, Photocatalytic performance of carbon-containing CuMo-based catalysts under sunlight illumination, Catalysts 12 (2022) 46.
[30] S. Malato, P. Fernández-Ibáñez, M.I. Maldonado, J. Blanco, W. Gernjak, Decontamination and disinfection of water by solar photocatalysis: Recent overview and trends, Catal. Today 147 (2009) 1–59.
[31] P. Fernández-Ibáñez, C. Sichel, M.I. Polo-López, M. de Cara-García, J. Tello, Photocatalytic disinfection of natural well water contaminated by Fusarium solani using TiO_2 slurry in solar CPC photoreactors, Catal. Today 144 (2009) 62–68.
[32] D.A. Keane, K.G. McGuigan, P. Fernández Ibáñez, M.I. Polo-López, J.A. Byrne, P. S.M. Dunlop, et al., Solar photocatalysis for water disinfection: Materials and reactor design. Catal, Sci. Technol. 4 (2014) 1211–1226.
[33] J. Matos, P. Atienzar, H. García, J.C.J. Hernández-Garrido, Nanocrystalline carbon–TiO_2 hybrid hollow spheres as possible electrodes for solar cells, Carbon 53 (2013) 169–181.
[34] J. Matos, C. Miranda, P.S. Poon, H.D. Mansilla, Nanostructured hybrid TiO_2-C for the photocatalytic conversion of phenol, Sol. Energy 134 (2016) 64–71.
[35] J. Matos, J. Ocares-Riquelme, P.S. Poon, R. Montaña, X. García, K. Campos, et al., C-doped anatase TiO_2: Adsorption kinetics and photocatalytic degradation of methylene blue and phenol, and correlations with DFT estimations, J. Coll. Inter. Sci. 547 (2019) 14–29.
[36] M.C. Fernández de Cordoba, J. Matos, R. Montaña, P.S. Poon, S. Lanfredi, F.R. Praxedes, et al., Sunlight photoactivity of rice husks-derived biogenic silica, Catal. Today 328 (2019) 125–135.
[37] F. Rouquerol, J. Rouquerol, K.S.W. Sing, P. Llewellyn, G. Maurin, Adsorption by Powders and Porous Solids: Principles, Methodology and Applications, 2nd Ed., Elsevier, Oxford, 2014.
[38] H.E. Swanson, R.K. Fuyat, Standard X-ray Diffraction Powder Patterns, National Bureau of Standards Circular 539 Volume II, 1954.
[39] H.E. Swanson, R.K. Fuyat, G.M. Ugrinic, Standard X-ray Diffraction Powder Patterns, National Bureau of Standards Circular 539 Volume III, 1954.
[40] J. Matos, S. Miralles-Cuevas, A. Ruíz-Delgado, I. Oller, S. Malato, Development of TiO_2-C photocatalysts for solar treatment of polluted water, Carbon 122 (2017) 361–373.
[41] Z. Kang, X. Yan, Y. Wang, Z. Bai, Y. Liu, Z. Zhang, et al., Electronic structure engineering of Cu_2O film/ZnO nanorods array all-oxide p-n heterostructure for enhanced photoelectrochemical property and self-powered biosensing application, Sci. Reports 5 (2015) 7882.
[42] G.D. Gesesse, A. Gomis-Berenguer, M. Barthe, C.O. Ania, On the analysis of diffuse reflectance measurements to estimate the optical properties of amorphous porous carbons and semiconductor/carbon catalysts, J. Photochem. Photobiol. A: Chem. 398 (2020) 112622–112632.
[43] C.H. Giles, D. Smith, A.J. Huitson, General treatment and classification of the solute adsorption isotherm, I. Theoretical. J. Coll. Inter. Sci. 47 (1974) 755–765.
[44] M. Sanchez, M.J. Rivero, I. Ortiz, Kinetics of dodecylbenzenesulphonate mineralisation by TiO_2 photocatalysis, Appl. Catal. B: Environ. 101 (2011) 515–521.
[45] E.D. Revellame, D.L. Fortela, W. Sharp, R. Hernandez, M.E. Zappi, Adsorption kinetic modeling using pseudo-first order and pseudo-second order rate laws: A review, Cleaner Engineering and Technology 1 (2020) 100032.
[46] M. Purnachander- Rao, J.J. Wu, A.M. Asiri, S. Anandan, Photocatalytic degradation of tartrazine dye using CuO straw-sheaf-like nanostructures, Water Sci. Technol. 75 (2017) 1421–1430.

[47] J.-M. Herrmann, Heterogeneous photocatalysis: Fundamentals and applications to the removal of various types of aqueous pollutants, Catal. Today 53 (1999) 115–129.
[48] N. Chekir, D. Tassalit, O. Benhabiles, N.K. Merzouk, M. Ghenna, A. Abdessemed, et al., A comparative study of tartrazine degradation using UV and solar fixed bed reactors, Inter. J. Hyd. Energy 42 (2017) 8948–8954.
[49] M.G. Popadić, S.R. Marinović, T.M. Mudrinić, A.D. Milutinović-Nikolić, P.T. Banković, I.S. Đorđević, et al., A novel approach in revealing mechanisms and particular step predictors of pH dependent tartrazine catalytic degradation in presence of Oxone®, Chemosphere 281 (2021) 130806.
[50] L. Ali, R. Algaithi, H.M. Habib, U. Souka, M.A. Rauf, S.S. Ashraf, Soybean peroxidase-mediated degradation of an azo dye–A detailed mechanistic study, BMC Biochem. 14 (2013) 35–47.
[51] L.H. Mendoza-Huizar, A theoretical study of chemical reactivity of tartrazine through DFT reactivity descriptors, J. Mex. Chem. Soc. 28 (2014) 416–423.
[52] G. Chen, L.C. Nengzi, Y. Gao, G. Zhu, J. Gou, X. Cheng, Degradation of tartrazine by peroxymonosulfate through magnetic Fe_2O_3/Mn_2O_3 composites activation, Chin. Chem. Lett. 31 (2020) 2730–2736.
[53] V. Ramasamy-Raja, D. Rani-Rosaline, A. Suganthia, M. Rajarajan, Facile sonochemical synthesis of Zn_2SnO_4-V_2O_5 nanocomposite as an effective photocatalyst for degradation of Eosin Yellow, Ultrason. Sonochemistry 44 (2018) 310–318.
[54] W.R. Abd-Ellatif, N.G. Mahmoud, A.A. Hashem, M.K. El-Aiashy, E.M. Ezzo, S.A. Mahmoud, Efficient photodegradation of E124 dye using two-dimensional Zn-Co LDH: Kinetic and thermodynamic studies, Environ. Technol. Innovation 27 (2022) 102393.
[55] N. John, R.N. Priyanka, T. Abraham, M.S. Punnoose, B.K. John, B. Mathew, Rational design of Ag_2CO_3-loaded SGO heterostructure with enhanced photocatalytic abatement of organic pollutants under visible light irradiation, Environ. Sci. Pollut. Res. (2022), https://doi.org/10.1007/s11356-022-19606-z.
[56] Y. Chen, S. Zhang, C. Jiang, T. Zhong, Z. Su, Q. Xu, et al., In-situ immobilization of titanium dioxide on poly (ether ether ketone) hollow fiber membranes and the effect of pH level on the photo-removal process of dyes, J. Mater. Sci. 57 (2022) (2022) 2483–2501.
[57] M.M. Sabzehmeidani, H. Karimi, M. Ghaedi, Enhanced visible light-active $CeO_2/CuO/Ag_2CrO_4$ ternary heterostructures based on CeO_2/CuO nanofiber heterojunctions for the simultaneous degradation of a binary mixture of dyes, New J. Chem. 44 (2020) 5033–5048.
[58] M.H. Barzegar, M. Ghaedi, V.M. Avargani, M.M. Sabzehmeidani, F. Sadeghfar, R. Jannesar, Electrochemical synthesis and efficient photocatalytic degradation of azo dye alizarin yellow R by Cu/CuO nanorods under visible LED light irradiation using experimental design methodology, Polyhedron 158 (2019) 506–514.